Kochi Chapter

Indian Geotechnical Conference
IGC 2022
15th – 17th December, 2022, Kochi

Assessment of Predictive Equations of Extents of Failure Zone in Sand beneath the Cutting Edge of Open Caisson using Image Analysis

Jitesh T. Chavda[1][0000-0003-0396-5759] and G. R. Dodagoudar[2][1111-2222-3333-4444]

[1]Department of Civil Engineering, Sardar Vallabhbhai National Institute of Technology Surat, Surat 395007, India
[2]Department of Civil Engineering, Indian Institute Technology Madras, Chennai 600036, India
jiteshchavda03@yahoo.in, goudar@iitm.ac.in

Abstract. Open caissons are classified as deep foundations. Caissons are sunk into the ground by removal of soil within the caisson shaft. A cutting edge with a tapered inner face is provided at the bottom of the caisson to allow the bearing failure of the soil. The bearing failure of soil results in the formation of influence zone which is termed as failure zone. In this study, the 1*g* caisson model tests on sand are carried out with different configuration of cutting edge i.e., varying radii ratio and different cutting angles and different sinking depth to evaluate the radial and vertical extents of failure zone. In the tests, the half-cut caisson models are penetrated in the sand and series of photos are captured. Using the captured photos, image analysis is performed to obtain the experimental failure zone. Based on the literature, the predictive equations to determine the extents of failure zone are assessed by comparing the extents of failure zone obtained from the experiments and the equations. The predictive equations help in quick estimation of the extent of failure zone based on the configuration of the open caisson adopted at the construction site.

Keywords: Open caisson, 1g model test, Cutting edge, Image analysis, Failure zone.

1 Introduction

The soil in contact with the cutting edge fails in bearing when the cutting edge of the caisson is loaded with the subsequent raising of the steining. The bearing failure leads to formation of influence zone termed as failure zone beneath the cutting edge. This bearing failure of soil initiates the sinking of the open caisson. The estimation of the vertical and radial extents of the failure zone and bearing capacity of the cutting edge will help in planning of proper excavation strategies to achieve the controlled sinking of the caisson.

The open caisson of larger diameter (i.e., $D_o > 10$ m) are generally used for launch and reception pits for tunnel boring machines and underground units like pumping stations, storm water tanks, storage and attenuation tanks (e.g., Nonveiller, 1987; Allenby *et al*., 2009; Yao *et al*., 2014; Royston *et al*., 2016; Sheil *et al*., 2018). Figure 1 shows the excavation of soil at the cutting edge of the large diameter caisson by machine

excavators. The sinking of such larger diameter caisson needs proper excavation strategies to allow the uniform sinking. The uneven sinking of the caisson may result in stress concentration and structural failure of the steining.

Fig. 1 Large diameter caisson for launch and reception pits for tunnel boring machines and underground units like pumping stations, storm water tanks, storage and attenuation tanks (Nonveiller, 1987; Allenby et al., 2009; Yao et al., 2014; Royston et al., 2016; Sheil et al., 2018)

In such cases, the sequential excavation is adopted for the uniform and control sinking of the caisson (see Fig. 2). A rough estimation of the extent of the influence zone in the soil based on the configuration of the cutting edge and the soil type helps in proper

planning of sequential excavation strategies (Nonveiller, 1987). The soil is excavated near the cutting edge in sequence as shown in the Fig. 2. This allows the failure of soil in contact with cutting edge altogether and permits uniform sinking. However, the guidelines on how much deeper and up to what radial extent the soil need to be excavated is limited. For estimation of the extent of influence zone in the soil beneath the cutting edge of the open caisson, Chavda and Dodagoudar (2018) have carried out sensitivity analysis and the extent of the failure zone corresponding to the various parameters is evaluated. The parameters considered in the sensitivity analysis are: radius ratio (r_i/r_o) and tapered angle (β) of the cutting edge, unit weight (γ), friction angle (ϕ), and cohesion of the soil (c), and magnitude of surcharge (q) representing depth of sinking of the caisson. The predictive equations are developed to estimate the extent of the failure zone for the given range of parameters and units as given in Table 1. The developed predictive equations are:

$$X/B = -0.9817 + 5.6522(r_i/r_o) - 0.0276(\beta) + 0.0374(c) + 0.0325(\phi) + 0.0028(q) - 0.0307(\gamma) \quad (1)$$

$$Y/B = 1.0596 + 1.5214(r_i/r_o) - 0.0167(\beta) + 0.0120(c) + 0.0101(\phi) + 0.0013(q) - 0.0093(\gamma) \quad (2)$$

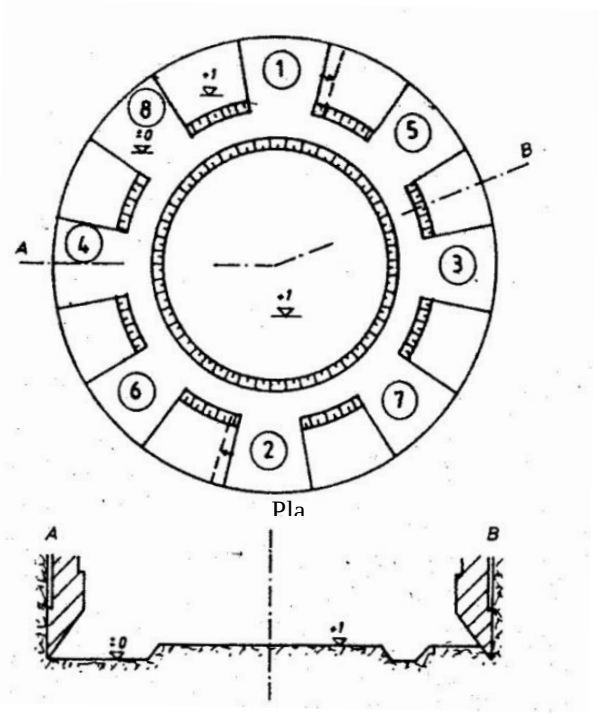

Pla

Section A-

Fig. 2 Excavation sequences, 1-8, for uniform sinking of caisson (Nonveiller, 1987)

The measurement of soil displacements in geotechnical experimentations using particle image velocimetry (PIV) technique is reported in the literature (White *et al*., 2003; Rechenmacher and Finno, 2004; Iskander, 2010; Take, 2015; Stanier *et al*., 2016; Xiao *et al*., 2017; Yuan *et al*., 2017, Chavda *et al*. 2019). The soil flow corresponding to the varying cutting angles of the cutting edge is evaluated using PIV technique by Royston *et al*. (2016). They performed the experiments corresponding to the plane strain condition, applicable for the circular open caisson with higher radius ratio, approximately equal to 1. The soil flow corresponding to the varying cutting angles, radii ratio and depth of sinking of the cutting edge is evaluated using open source MATLAB module, GeoPIV-RG has been reported by Chavda *et al*. (2019). The module GeoPIV-RG follows the principles of PIV, originally developed in the field of experimental fluid mechanics (Adrian, 1991). Certain modifications to the PIV technique have been proposed by White *et al*. (2003) and Stanier *et al*. (2016) to enhance its applicability in geotechnical engineering.

Table 1 Range of parameters used in the regression (Chavda and Dodagoudar 2019)

Component	Parameter	Unit	Range
Soil	γ	kN/m^3	14 - 22
	c	kPa	0 - 30
	ϕ	degree	5 - 30
Geometry of cutting edge	r_i/r_o	-	0.5 - 0.9
	β	degree	30 - 90
Surcharge	q	kPa	0 - 150

In the present study, the soil displacements around the cutting edge of the circular open caissons with different cutting angles have been investigated by performing the image-based deformation analysis using GeoPIV-RG. The failure zones in the sand at the cutting edge of the circular open caisson are evaluated using 1g model test. The extent of failure zone in sand corresponding to the cutting edge with different radii ratios, varying cutting angles and different sinking depths are evaluated using image-based deformation measurement technique. The results obtained from the 1g model half-open caisson tests are used to assess the predictive equations (Eqs. 1 and 2). The extent of the failure zone obtained from the experiments is compared with the extent of the failure zone obtained from the predictive equations. The results of the present study provide a clear picture of the extent of the failure zone around the cutting edge.

2 Experimental Program

2.1 Test Setup and Sand used in the study

The loading frame used for CBR test is used for the evaluation of soil flow mechanism (See Fig. 3). The tank is fabricated with one side transparent, also termed as a viewing window, to capture the soil movement around the cutting edge of the half-open caisson during the penetration. The Indian standard (IS) sand, properties reported in Table 2, is used in the model tests (IS: 650, 1991). All tests are performed at relative density of the sand at D_r = 50% to limit the scope of the study to one density.

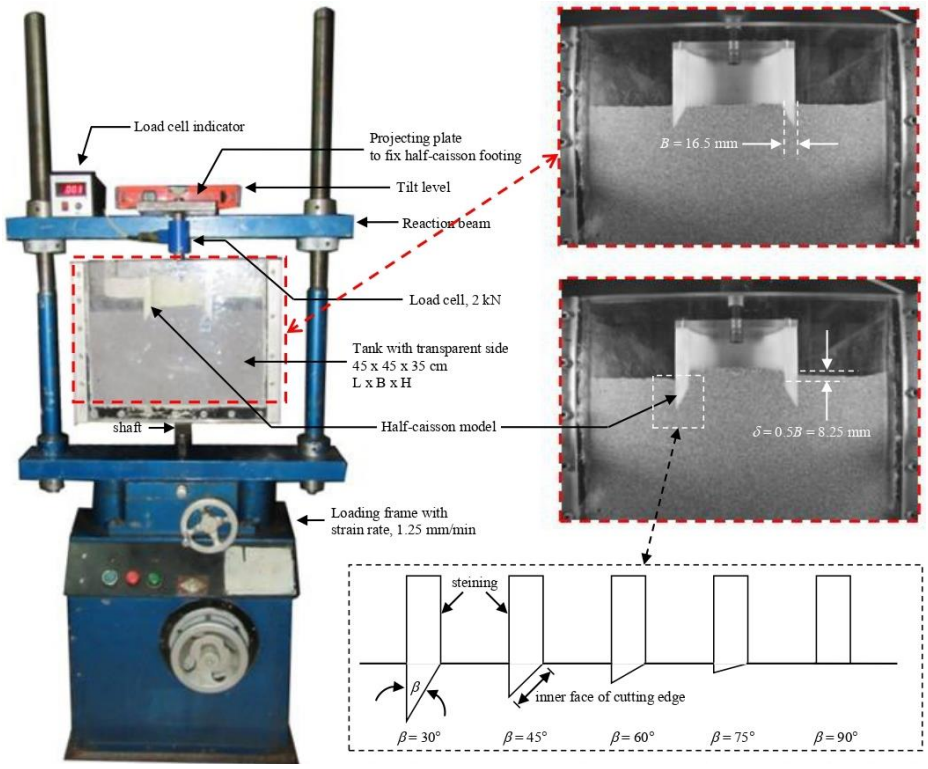

Fig. 3 Experimental set-up of half-open caisson model showing loading frame, closer view of viewing window of the tank, and configuration of the cutting edge of the half-open caisson

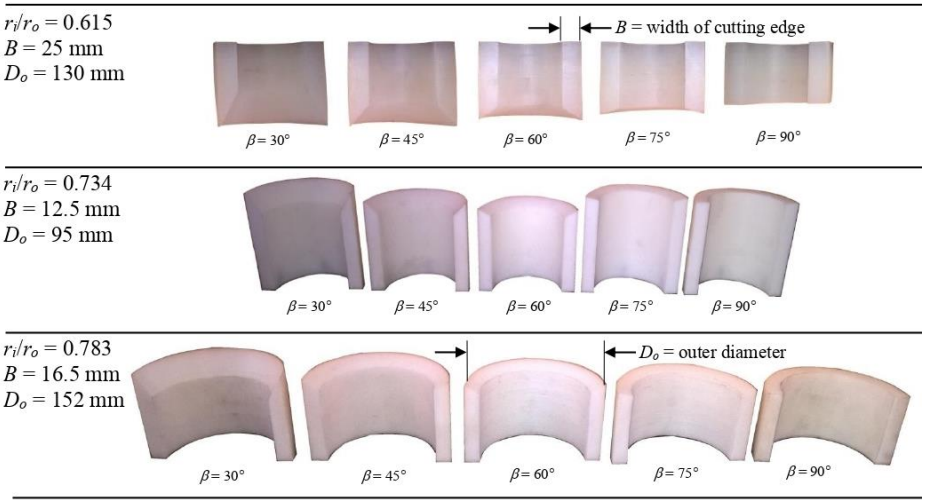

Fig. 4 Configuration of the half-open caisson models

Table 2 Index properties of Indian standard sand (Grade II)

Parameter	Unit	Value	Reference
Specific gravity	-	2.64	ASTM (2016a)
Max. unit weight	kN/m^3	16.81	ASTM (2016a)
Min. unit weight	kN/m^3	14.50	ASTM (2016b): Method B
Relative density	%	50	ASTM (2016b)
Unit weight of sand	kN/m^3	15.57	ASTM (2016a)
ϕ (D_r = 50%)	degree	35°	IS: 2720-13 (1996)
ψ (D_r = 50%)	degree	11°	IS: 2720-13 (1996)
Young's modulus	MPa	5.768	Plate load test
Poisson's ratio	-	0.3	$K_0 = 1 - sin(\phi)$
Height of fall (D_r = 50%)	mm	270	ASTM (2016b)
Unified soil classification	-	SP[a]	ASTM (2011)

[a]SP - Poorly graded sand

For the image-based deformation measurement analysis, the sand texture has been optimized to maximize the precision in the measurement of the soil displacements (White *et al.*, 2003; Take, 2003; White and Take, 2005; Stanier and White, 2013). White *et al.* (2003) reported that the natural texture present in the river sand is sufficient to carry out the image analysis. However, the sand used in the present study has an off-white color. Hence, artificial seeding is necessary to achieve the required texture in the sample. The procedure and methodology reported in Chavda *et al.* (2019) is used for the preparation of the dyed sand and the optimum texture respectively. The dyed sand was prepared by mixing 60 ml of black colour pen ink with 5 kg of sand. Then the sand was kept in an oven at 105 °C for 24 hr so that the colour is absorbed by the sand particles. In order to remove the excess ink, the dyed sand was washed with the fresh water and kept in the oven for another 24 hr to remove the moisture. The black coloured dyed sand thus obtained is termed as the seeding sand in the present study. The texture in the sand is generated by mixing the IS sand and seeding sand at 65% and 35% by weight. The sand used in all the experiments is seeded with 65% of the dyed sand i.e., it comprises of 35% of the natural sand and 65% of the dyed sand by weight to achieve the required texture.

Table 3 Properties of caisson model

Material	Parameter	Unit	Value
Caisson model: Polytetrafluoroethylene	Unit weight	kN/m^3	11
	Young's modulus	MPa	500
	Poisson's ratio	-	0.46

2.2 Caisson Models

For the image analysis, the caisson models are half cut to represent an axisymmetric problem. The configuration of the half-cut open caisson models are depicted in Fig. 4. The half-open caisson models are fabricated from the Polytetrafluoroethylene (PTFE) Teflon tubes. The transparent side of the tank is made of Perspex acrylic sheet. For maximum repetitive use of the transparent acrylic glass, the half-open caisson models are fabricated with PTFE for the investigation of the soil flow mechanism. The

properties of the PTFE caisson models are given in Table 3. The Young's modulus of the PTFE is almost 80 times higher than the sand and hence the half-cut caisson models are relatively rigid and hence they experience negligible deformations.

2.3 Data Processing

The images obtained from the tests consist of series of images from the initial to the final penetration depth same as the width of the cutting edge. In any PIV analysis, the deformations at any point of time are calculated using a particular image by comparing it to the reference image (initial undeformed image). The reference image represents the image corresponds to zero penetration of the caisson and the final image represents the image corresponds to the particular penetration at which the displacement field of the sand medium is required to be evaluated. In the study, the depth of penetration is kept same as half the width of the cutting edge. At this penetration, the fully developed failure envelops are obtained.

2.4 Camera and Test Procedure

In the present study, a Nikon D5300 digital single-lens reflex (DSLR) camera, with AF-S NIKKOR lens, f/3.5- 5.6, 18-55 mm focal length, is used which employs a complementary metal-oxide-semiconductor (CMOS) sensor (23.5 mm×15.6 mm) with a rolling shutter arrangement. The use of such camera in large deformation analysis has already been reported by Mishra *et al.* (2017), in measuring localised strains in geotextiles. In order to compensate for the low optical sensitivity of the CMOS sensor and to reduce the shutter speed, an external lighting is provided by the two 16W LED light panels. The test is performed by moving the tank in the upward direction with a constant strain rate of 1.25 mm/min and the photographs are captured at an interval of 3 seconds (0.33 Hz). This frequency of image acquisition is decided based on the strain rate and displacement of the soil medium between the two successive images.

3 Results and Discussion

3.1 Assessment of the Predictive Equations

The results of the image analysis corresponding to the varying radii ratio (r_i/r_o= 0.613, 0.743 and 0.783) and tapered angles of the cutting edge (β = 30°, 45°, 60°, 75° and 90°) are used to assess the predictive equations. The vectorial and horizontal displacement plots corresponding to the penetration depth of 0.5B are obtained from the GeoPIV_RG program for r_i/r_o = 0.613, 0.743 and 0.783.

In the horizontal displacement contour plot, in order to identify the clear picture of the failure zone, only the radially inward horizontal displacement vectors are shown. The typical plot of the vectorial displacement, horizontal displacement contours, and radially inward displacement contours are shown in Fig. 5 corresponding to the cutting edge having a radius ratio of 0.783 and a cutting angle of 60°. The extent of the failure zone is evaluated from these plots for varying radii ratio and cutting angles. Equations (1) and (2) are used to predict the extent of the failure zone for the same configuration

of the cutting edge and material properties of the sand as used in the tests. The experimental values and those predicted from the equations are compared and shown in Fig. 6. It is observed from the figure that Eqs. (1) and (2) estimated the extent of the failure zone within 20% of the error band. The error band of 20% is with respect to the value of X/B = Y/B = 4. These predictive equations can be used to identify the extent of the failure zone in the field and accordingly the suitable excavation strategies can be adopted.

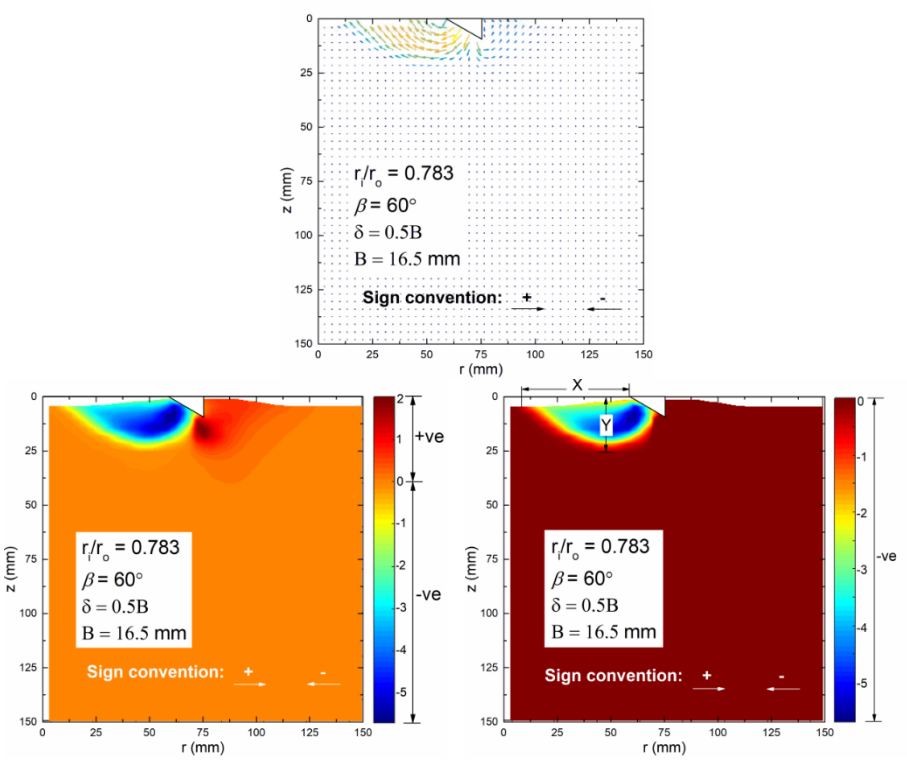

Fig. 5 Typical vectorial displacements, horizontal displacement contours, and radially inward displacement contours (Chavda and Dodagoudar, 2019)

4 Conclusions

In the study, the predictive equation to estimate size of failure zone in soil beneath the cutting edge of open caisson is examined. The equation accounts the effect of variation of geometry of the cutting edge, soil properties, and depth of sinking on the extents of the failure zone. The experimental results from the 1*g* caisson tests are used to assess the predictive equations. The predictive equations can be used in the preliminary estimation of the extent of the failure zone in the radial and vertical directions for the selected configuration of the open caisson. Following conclusions are drawn from the present study:

- The easy-to-use predictive equations have been assessed to estimate the radial and vertical extent of the failure zone in the soil beneath the cutting edge of the open caisson. The extent of the failure zone is determined from the 1*g* caisson tests and is compared with the estimated extent of the failure zone from the predictive equations. The predictions made by the equations are within 20% error band of the experimental results.
- Based on the assessment, the predictive equation can be used as the guidelines on how much deeper and up to what radial extent the soil need to be excavated for controlled and uniform sinking of large diameter caisson with confidence.

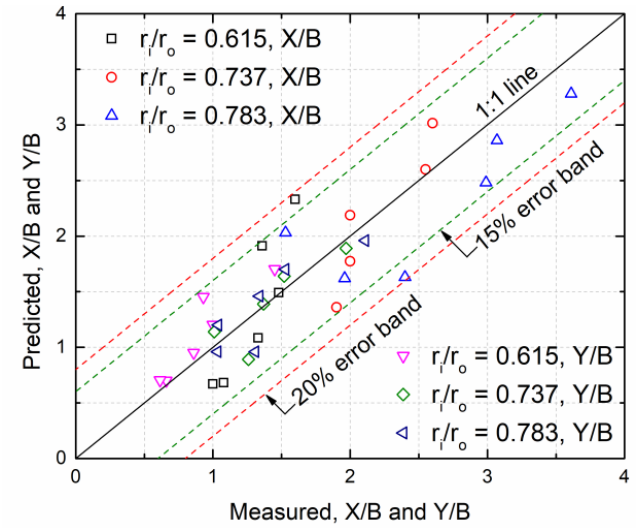

Fig. 6 Comparison of experimental results and predicted values of the extent of failure zone at the cutting edge

References

1. Adrian, R. J. (1991) Particle imaging techniques for experimental fluid mechanics. *Annual Review of Fluid Mechanics*, 23, 261–304.
2. Allenby, D., G. Waley and D. Kilburn (2009) Examples of open caisson sinking in Scotland. *Proceedings of the ICE - Geotechnical Engineering*, 162(1), 59-70.
3. ASTM (2016a) Standard test methods for maximum index density and unit weight of soils using a vibratory table. ASTM D4253-16, West Conshohocken, PA.
4. ASTM (2016b) Standard test methods for minimum index density and unit weight of soils and calculation of relative density. ASTM D4254-16, West Conshohocken, PA.
5. ASTM (2011) Standard practice for classification of soils for engineering purposes (unified soil classification system) ASTM D2487-11, West Conshohocken, PA.
6. Chavda, J. T. and G. R. Dodagoudar (2018). Finite element modelling of extent of failure zone in *c*-φ soil at the cutting edge of open caisson. *Numerical Methods in Geotechnical Engineering IX: Proceedings of the 9th European Conference on Numerical Methods in Geotechnical Engineering*, Porto, Portugal, 25 - 27th June 2018.
7. Chavda, J. T., S. R. Mishra and G. R. Dodagoudar (2019) Experimental evaluation of ultimate bearing capacity of the cutting edge of open caisson, *International Journal of Physical Modelling in Geotechnics*, doi: 10.1680/jphmg.18.00052.

8. Chavda, J. T. and G. R. Dodagoudar (2019). Experimental evaluation of failure zone in sand beneath the ring footing and cutting edge of open caisson using image analysis. *Indian Geotechnical Conference 2019*, SVNIT Surat, Gujarat, India, December 2019.
9. Iskander, M. (2010) *Modelling with Transparent Soils Visualizing Soil Structure Interaction and Multi Phase Flow, Non-Intrusively*. Springer, New York.
10. IS: 650 (1991) Standard sand for testing cement - Specification. Bureau of Indian Standards, New Delhi.
11. IS: 2720-13 (1996) Methods of test for soils, Part 13: Direct shear test. Bureau of Indian Standards, New Delhi.
12. Mishra, S. R., S. R. Mohapatra, N. Sudarsanan, K. Rajagopal and R. G. Robinson (2017) A simple image-based deformation measurement technique in tensile testing of geotextiles. *Geosynthetics International*, 24(3), 306-320.
13. Nonveiller, E. (1987) Open caissons for deep foundations. *Journal of Geotechnical Engineering*, ASCE, 113(5), 424-439.
14. Royston, R., B. M. Phillips, B. B. Sheil and B.W. Byrne (2016) Bearing capacity beneath tapered edges of open dug caissons in sand. *Proceedings of Civil Engineering Research in Ireland*, Galway, Ireland.
15. Rechenmacher, A. L. and R. J. Finno (2004) Digital image correlation to evaluate shear banding in dilative sands. *Geotechnical Testing Journal*, 27(1), 13–22.
16. Stanier, S. A., J. Blaber, W. A. Take and D. J. White (2016) Improved image-based deformation measurement for geotechnical applications. *Canadian Geotechnical Journal*, 53(5), 727–739.
17. Stanier, S. A. and D. J. White (2013) Improved image-based deformation measurement for the centrifuge environment. *Geotechnical Testing Journal*, 36(6), 915-927.
18. Sheil B., R. Royston and B. Byrne (2018) Real-time monitoring of large-diameter caissons. *Proceedings of China-Europe Conference on Geotechnical Engineering*, 725-729, https://doi.org/10.1007/978-3-319-97112-4_162.
19. Take, W. A. (2015) Thirty-Sixth Canadian Geotechnical Colloquium: Advances in visualization of geotechnical processes through digital image correlation. *Canadian Geotechnical Journal*, 52(9), 1199–1220.
20. Take, W. (2003) The influence of seasonal moisture cycles on clay slopes, Ph.D. Thesis, University of Cambridge, Cambridge, U.K.
21. White, D. J., W. A. Take and M. D. Bolton (2003) Soil deformation measurement using particle image velocimetry (PIV) and photogrammetry. *Géotechnique*, 53(7), 619-631.
22. Yuan, B., K. Xu, Y. Wang, R. Chen and Q. Luo (2017) Investigation of deflection of a laterally loaded pile and soil deformation using the PIV technique. *International Journal of Geomechanics*, ASCE, 17(6), 04016138, 1-9.
23. Xiao, Y., F. Yin, H. Liu, J. Chu and W. Zhang (2017) Model tests on soil movement during the installation of piles in transparent granular soil. *International Journal of Geomechanics*, ASCE, 17(4), 06016027, 1-7.
24. Yao, Q., X. Yang and H. Li (2014) Construction technology of open caisson for oversize surge shaft in drift gravel stratum, *Electronic Journal of Geotechnical Engineering*, 19, 5725-5738.
25. White, D. J. and W. A. Take (2005) Discussion on: Application of particle image velocimetry (PIV) in centrifuge testing of uniform clay by Zhang Y. D., Tan T. S. and Leung C. F. *International Journal of Physical Modelling in Geotechnics*, 5(4), 27-31.